1997

Multiband photometry of rich abell clusters: constraints on the dwarf star content of dark matter

Stephen P. Boughn
Haverford College, sboughn@haverford.edu

J. M. Uson

THE ASTROPHYSICAL JOURNAL, 488:44–54, 1997 October 10

MULTIBAND PHOTOMETRY OF RICH ABELL CLUSTERS: CONSTRAINTS ON THE DWARF STAR CONTENT OF DARK MATTER

STEPHEN P. BOUGHN[1]
Department of Astronomy, Haverford College, Haverford, PA 19041 and Institute for Advanced Study, Princeton, NJ 08540
AND
JUAN M. USON[1]
National Radio Astronomy Observatory,[2] 520 Edgemont Road, Charlottesville, VA 22903
Received 1995 October 31; accepted 1997 May 13

ABSTRACT

We present results of large-aperture ($\sim 1'$) *JK* photometry and CCD *BVRI* photometry near the centers of three distant ($0.11 \leq z \leq 0.22$), rich Abell clusters of galaxies. The colors of the integrated light are consistent with those of nearby E and S0 galaxies. The absence of anomalous reddening implies that no more than $2\ h^{-1}\%$ (1 σ limit) of the dark matter in these clusters can be in the form of low-mass ($\sim 0.1\ M_\odot$) subdwarfs or old disk dwarfs. The limit increases to $3\ h^{-1}\%$ if expressed in terms of zero-metallicity dwarfs. These results constrain the mass function of baryonic objects which might contribute to the dark matter.

Subject headings: dark matter — galaxies: clusters: general — galaxies: photometry — galaxies: stellar content — stars: late-type

1. INTRODUCTION

The mass required to bind galaxies and clusters of galaxies usually exceeds the total mass in stars and gas by up to 2 orders of magnitude. This is the well-known "dark matter" problem (Zwicky 1933; Faber & Gallagher 1979). The nature of the dark matter remains one of the most important unsolved problems of astronomy. A number of rather exotic solutions to this problem have been suggested such as a variety of hypothetical weakly interacting massive particles (none of which has ever been detected) and populations of collapsed objects, e.g., primordial black holes (Peebles 1993). Perhaps the most conservative model for the dark matter is a population of red and/or brown dwarf stars which are so faint that they have escaped detection. Brown dwarfs, stars with masses too small ($<0.1\ M_\odot$) to support significant hydrogen fusion, are hard to detect outside the solar neighborhood. A few candidates have been recently detected in nearby star clusters (see Rebolo, Zapatero Osorio, & Martin 1995; Zapatero Osorio, Martin, & Rebolo 1997; Festin 1997). Their numbers are so far consistent with smooth extensions of the stellar mass functions of those clusters. The faintest main-sequence stars are considerably brighter though most of the light from these stars is emitted in the infrared (IR) bands. A population of such stars has been the primary target of searches for dark matter in the IR bands (Boughn & Saulson 1983; Skrutskie, Shure, & Beckwith 1985).

Recent *Hubble Space Telescope* observations of the halo of the Galaxy indicate that ($<1\%$) of the mass of the Galactic halo can be in the form of low-mass stars (Flynn, Gould, & Bahcall 1996; Graff & Freese 1996). On the other hand, Sackett et al. (1994) have reported a component of diffuse *R*-band light around the edge-on spiral galaxy NGC 5907. The profile of the light falls off more slowly than the known exponential component for spirals and is consistent with the distribution of dark matter in that galaxy with a mass-to-light ratio of ~ 450 in solar *R*-band units, comparable to that of stars near the edge of the main sequence. The colors of this diffuse light, however, are only slightly redder than the disk (Lequeux et al. 1996) and, therefore, much too blue to be due to faint dwarf stars. This leaves open the possibility that the diffuse light may be due to a relatively low-mass ($\leq 0.8\ M_\odot$) population of stars which simply trace the otherwise dark halo mass.

The mass-to-light ratios of rich clusters of galaxies are about 10 times larger than those of individual galaxies; therefore, observations of clusters are likely to be more sensitive probes of the dark matter. In addition, there is no guarantee that the cluster dark matter has the same composition as the dark matter in the halos of individual galaxies. Indeed, strong constraints on the red dwarf content of dark matter have come from observations of diffuse infrared light in four Abell clusters of galaxies (Uson & Boughn 1991, hereafter UB91). Those observations indicated that less than $5\ h^{-1}\%$ of the dark matter in those clusters can be in the form of Population I red dwarf stars with masses $\sim 0.1\ M_\odot$ ($h = H_0/100$ km s^{-1} Mpc^{-1}, where H_0 is Hubble's constant). This limit is statistical in nature as the mass-to-light ratios derived from the individual measurements depend on the actual distribution of the matter in the clusters, which is not known in detail. The observations described in this paper extend the observations to seven Abell clusters and double the number of observed regions. In addition, the analysis is extended to include populations of low- and zero-metallicity stars which are, perhaps, more reasonable models for the constituents of the dark matter. Similar optical observations of a single cD cluster, Abell 2029, yielded a somewhat stronger limit, i.e., $\leq 1\%$ of the

[1] Visiting Astronomer at Kitt Peak National Observatory, National Optical Astronomy Observatories, operated by Association of Universities for Research in Astronomy, Inc., under contract with the National Science Foundation.

[2] The National Radio Astronomy Observatory is a facility of the National Science Foundation operated under cooperative agreement by Associated Universities, Inc.

dwarf star content of the dark matter in that cluster can be in the form of 0.1 $M_\odot$ solar metallicity dwarfs (Boughn & Uson 1995a, 1995b).

2. OBSERVATIONS

We obtained single-aperture J and K and CCD B-, V-, R-, and I-band photometry of nine positions at and near the dynamical centers of Abell clusters A115, A403, and A2397. We located the center of A403 and A2397 using the corresponding Palomar Observatory Sky Survey red plate. A115 is a cluster which shows substructure in both the X-ray emission and the galaxy distribution and was studied in depth by Beers, Huchra, & Geller (1983). We observed the southern clump (B in their paper). The off-center positions were chosen to be devoid of bright cluster galaxies or foreground stars.

2.1. *BVRI Observations*

We obtained *BVRI* (Mould filter set) CCD photometry on the cores of these clusters with the No. 1, 0.9 m telescope at KPNO. We used the 348 × 512 RCA No. 2 chip on the first two nights and the RCA No. 1 chip on the third night. Both cameras had a scale of 0.″86 pixel^{-1}. The seeing was between 1.″0 and 1.″5. Each observation of a cluster in any given band consisted of a sequence of eight frames, with an integration time of 5 minutes per frame. The sequence began with two observations of a "blank" area followed by four observations of the cluster center with two observations of a second blank area to end the sequence. The telescope was offset by about 30″ between each exposure of a given area, which for the observations of the cluster resulted in a diamond pattern. The cluster exposures contained both the "center" and "off" positions. All the blank areas obtained for a band on a given night were used to generate a "sky flat" frame for that band as described below.

We observed stars of different spectral types of 10th–12th magnitude from Landolt's list of standard stars (Landolt 1983). These were used to determine atmospheric (secant law) and color corrections. All measurements were consistent with the calibration curves to within 0.02 mag.

We subtracted the bias level from each picture and trimmed them to a size of 316 × 508 pixels and subsequently divided them by standard dome flats. All the exposures of blank positions were stacked in order to identify "hot" pixels (several hundred). These were then eliminated from further analysis.

The reduction of each set of exposures for every band proceeded as follows. Each "blank" frame (at least 12 were available for each band) was submitted to a robust 2.5 σ filter (four iterations). Any region which consisted of three or more contiguous noncolinear pixels was designated an object and after determining its centroid and rms radius, all the pixels within 3.5 times the rms radius of the centroid of the object were also flagged. This was done in order to avoid contamination from the fuzz around galaxies and stars which would escape the 2.5 σ filtering. All so-cleaned frames (between 12 and 16) were averaged to form a "sky-flat" frame for each band. Any pixel which was not represented in at least eight individual frames was designated "bad" and flagged. All frames were then flattened by division with the composite sky flat. No residual structure other than objects was left in the flattened frames to less than 10^{-3} of the night sky.

The four cluster frames obtained for each band were registered and tesselated as described in UB91. The sky level varied by less than 7% during the observations, mostly due to the change in elevation. Offsets between overlapping frames were computed by comparing the average sky level in the overlap region of the corresponding frames after excluding objects using the procedure described above (robust filtering followed by [spatial] scaling of the objects found). Finally, overlapping frames were averaged. The non-overlapping regions were discarded which resulted typically in a loss of less than 8% of the pixels. Cosmic-ray hits were found by comparing the various measurements of any given sky position in an automated way.

2.2. *JK Observations*

We obtained single-aperture (61″) photometry in the J (1.25 μm) and K (2.2 μm) bands using the InSb photometer (Otto) at the Cassegrain focus of the KPNO 1.3 m telescope. We used the nutating secondary to switch the beam at a rate of 10 Hz. In order to eliminate offsets, we used a double-beam-switching scheme in which the target positions were alternatively compared with two reference positions on opposite sides of the target. Each of the single-switching observations lasted one minute. The beam throws were between 7′ and 11′, and the parallactic angles were chosen so that the reference positions were devoid of stars and galaxies on the corresponding Palomar plates. We scanned the apertures along the north-south and east-west directions in both the target and reference positions for several beam throws in order to determine the beam profiles. We scanned the telescope through the positions of bright stars while beam switching in the same way as was done during the actual observations and recorded the output of the synchronous detector with a strip-chart recorder. The tracings were consistent with circular apertures and provided us with effective "beam maps."

J and K-band KPNO infrared standard stars were observed at several zenith angles. A secant law was fitted to each night's data, and the resultant atmospheric extinction removed from the data. These corrections amounted to, at most, 0.1 mag. Because the beam throws were large, the change in airglow due to the secant-law atmospheric contribution resulted in a small but nonnegligible contribution to the signal. Airglow was determined by monitoring the DC channel of the photometer at several zenith angles, and this value was used to correct the data. Although these corrections were, in all cases, smaller than the standard deviations listed in Table 1 we chose to make them because they were nonrandom as well as predictable.

2.3. *Photometry*

The *JK* photometry for each cluster position are listed in Table 1. The quoted errors were derived from the data and include a contribution from residual electronic drifts in the InSb photometer. Other errors are estimated below.

In order to relate the *BVRI* observations to the single-aperture photometry used in the *JK* measurements, we convolved the composite CCD frames with aperture masks at the positions of the main and reference IR beams. These masks were constructed to match the measured beam patterns of the (switching) infrared beams discussed in the previous section. The beams were located by identifying stars in the CCD frames that corresponded to those visible to the automatic guider on the 1.3 m telescope to which the infra-

TABLE 1

PHOTOMETRY OF CLUSTER POSITIONS

Positions	$\Delta_{RA}, \Delta_{decl}$[a] (arcsec)	B	V	R	I	J	K
A115 No. 1	0, 0	17.59 ± 0.04	16.18 ± 0.02	15.52 ± 0.01	14.82 ± 0.02	13.69 ± 0.10	12.29 ± 0.07
A115 No. 2	28, 54	$19.71^{+0.33}_{-0.25}$	$18.71^{+0.20}_{-0.17}$	$18.35^{+0.22}_{-0.18}$	$18.95^{+\infty}_{-0.75}$	>16.02[b]	>15.19[b]
A115 No. 3	36, −28	18.54 ± 0.10	17.24 ± 0.04	16.78 ± 0.04	15.93 ± 0.06	$16.56^{+3.20}_{-0.72}$	$14.38^{+0.60}_{-0.39}$
A403 No. 1	4, −10	16.73 ± 0.02	15.34 ± 0.01	14.69 ± 0.01	14.03 ± 0.01	12.63 ± 0.05	11.63 ± 0.06
A403 No. 2	−32, 47	$18.98^{+0.16}_{-0.14}$	$18.02^{+0.12}_{-0.10}$	17.22 ± 0.05	$16.60^{+0.14}_{-0.12}$	$15.52^{+0.71}_{-0.43}$	$13.82^{+0.70}_{-0.42}$
A403 No. 3	64, 70	$18.84^{+0.16}_{-0.14}$	$18.75^{+0.21}_{-0.19}$	>20.54[b]	$21.20^{+\infty}_{-2.32}$	$15.52^{+0.86}_{-0.47}$	>14.29[b]
A403 No. 4	7, −88	>21.35[b]	$18.44^{+0.17}_{-0.14}$	17.13 ± 0.04	$18.23^{+0.84}_{-0.47}$	$15.69^{+0.91}_{-0.49}$	$13.16^{+0.21}_{-0.17}$
A2397 No. 1.....	−75, 19	>21.20[b]	$18.80^{+0.28}_{-0.21}$	$17.97^{+0.16}_{-0.14}$	$17.53^{+0.22}_{-0.19}$	$14.63^{+0.23}_{-0.19}$	$13.81^{0.34}_{-0.26}$
A2397 No. 2.....	46, 58	$20.66^{+1.03}_{-0.51}$	$17.90^{+0.12}_{-0.10}$	16.89 ± 0.05	15.56 ± 0.03	$14.50^{+0.26}_{-0.20}$	$13.28^{+0.32}_{-0.24}$

[a] Distance from nominal (dynamical) cluster center. For A115, we locate it at the position of the dominant galaxy of clump B of Beers et al. (1983) at R.A. = $0^h53^m18^s$, decl. = 26°04′19″. For A403 and A2397 the offsets are measured with respect to the respective cD galaxies (positive offsets correspond to displacements to the east and north).

[b] Corresponds to 1 σ or the measured value + 1 σ if the signal was positive. No signal was less than $-0.95\ \sigma$.

red beams were referred. We used positions in which several stars were visible to the guider in order to calibrate it in both orthogonal directions. We believe that we know the positions of the infrared apertures to within 1″. The R-band mosaics are shown in Figure 1 with location of the IR apertures.

The sky background in each mosaic was determined from the pixel intensity distribution. Histograms of number of pixels versus intensity were constructed from the data in each mosaic, after excluding the areas covered by the infrared beams. Gaussians were then fitted to these distributions and the procedure iterated to exclude pixels whose intensity exceeded the average by more than 1 σ in order to avoid a bias due to faint objects or the extended halos of bright objects. The mean of each fitted Gaussian was taken to be the corresponding background level of the night sky. This method provides a simple way to estimate a sky background which is largely insensitive to objects with intensities greater than the shot noise in the night sky, which is sufficiently accurate for our purposes. Pixels nearer than 150″ from the cluster center were excluded in order to avoid a possible contamination due to a diffuse component which might be present near the cluster center.

The values for the $BVRI$ photometry are also listed in Table 1. The quoted errors are derived from the data but include the contributions of errors due to the flat-fielding procedure. Data obtained for A403 in the R band on two different nights agreed to within the errors.

3. CLUSTER COLORS

3.1. *K-Corrections*

K-corrections are important because the observed clusters have redshifts between 0.11 and 0.22. Unfortunately, the corrections depend on the spectral distribution of the emitted light which is unknown. Since our observations were confined to the cores of rich clusters, most of the galaxies in the beams should be either ellipticals or early-type spirals. Therefore, we computed K-corrections assuming that the emitted light has the spectrum of a typical elliptical galaxy. We used the composite spectrum of Lebofsky & Rieke (Eisenhardt 1984) in the infrared and the standard elliptical spectrum of Yee & Oke (1978) in the visible. Table 2 lists the K-corrections which were computed using an open ($q_0 = 0$) universe. These change somwewhat for different values of q_0 but have no effect on the corrected colors and only a small one on the derived mass-to-light ratios as discussed below.

The central wavelengths of the observed R and V bands correspond roughly to those of the V and B bands in the cluster rest frames. Therefore, we correct the observed R- and V-band magnitudes to the rest-frame V and B magnitudes using the modified K-corrections that we introduced and discussed in detail in UB91. These two-band K-corrections are less sensitive to the spectrum of the observed light. We estimate that the uncertainties in the values in Table 2 are 0.05 mag even if the observed positions contain a nonnegligible fraction of late galaxies.

The K-corrections for red dwarfs differ significantly from those listed in Table 2. In our analysis (§ 4.2) we use color information to separate the standard galaxy contribution from that of the residual diffuse light. This requires an assumption for the spectral distribution of the light from such a component. We have analyzed the data assuming three different models of low-mass (0.1 $M_\odot$) dwarfs, i.e., old disk dwarfs, subdwarfs, and zero-metallicity dwarfs.

3.2. *Corrected Colors*

The corrected colors for the cluster positions are listed in Table 3 along with the average colors obtained from a survey of nearby E/S0 galaxies (Aaronson 1977; Frogel et al. 1978; Persson, Frogel, & Aaronson 1979; Aaronson, Persson, & Frogel 1981). Also listed in Table 3 are the colors of four Abell clusters reported in UB91. The survey colors were corrected slightly (≤ 0.1 mag) to take into account the radial color gradients reported by Frogel et al. (1978). All colors were corrected to one de Vaucouleurs radius. The errors listed are a quadrature combination of the statistical errors and 0.08 mag which accounts for any uncertainties in calibration and the K-corrections discussed above. The uncertainties listed in the last row reflect the

TABLE 2

K-CORRECTIONS

Cluster	K	J	$R \rightarrow V$	$V \rightarrow B$
A115	−0.42	−0.05	−0.33	−0.52
A403	−0.25	−0.08	−0.45	−0.68
A2397.....	−0.48	−0.05	−0.29	−0.44

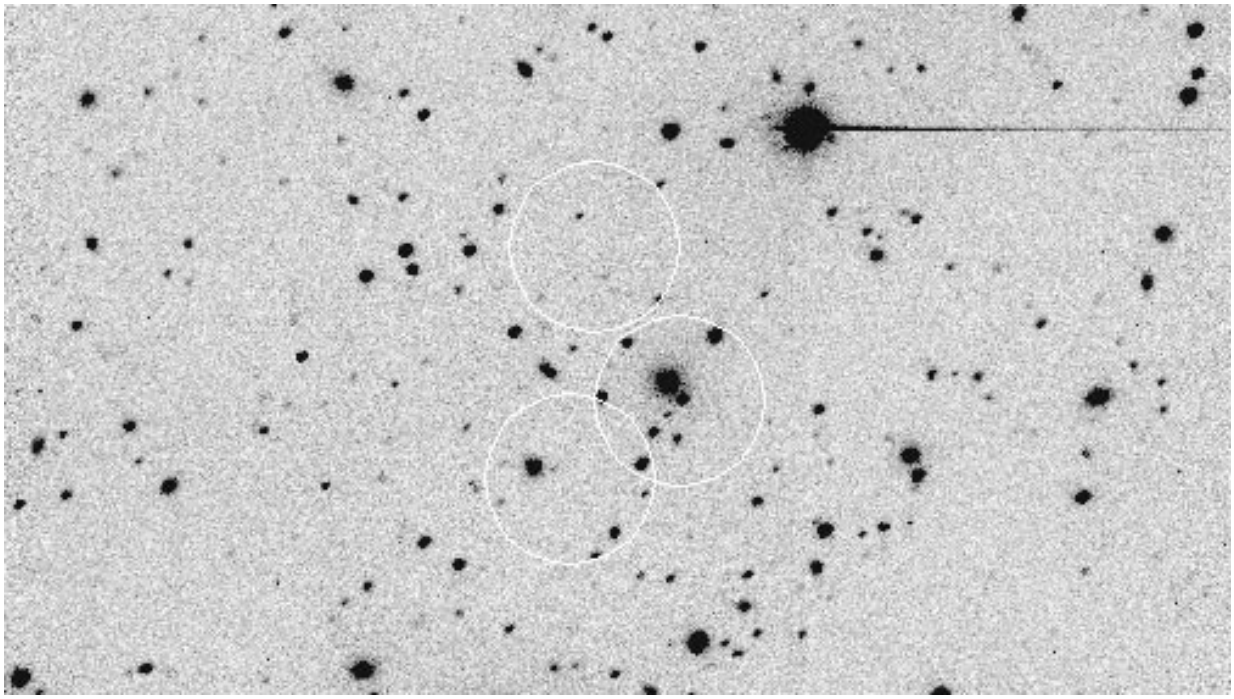

FIG. 1*a*

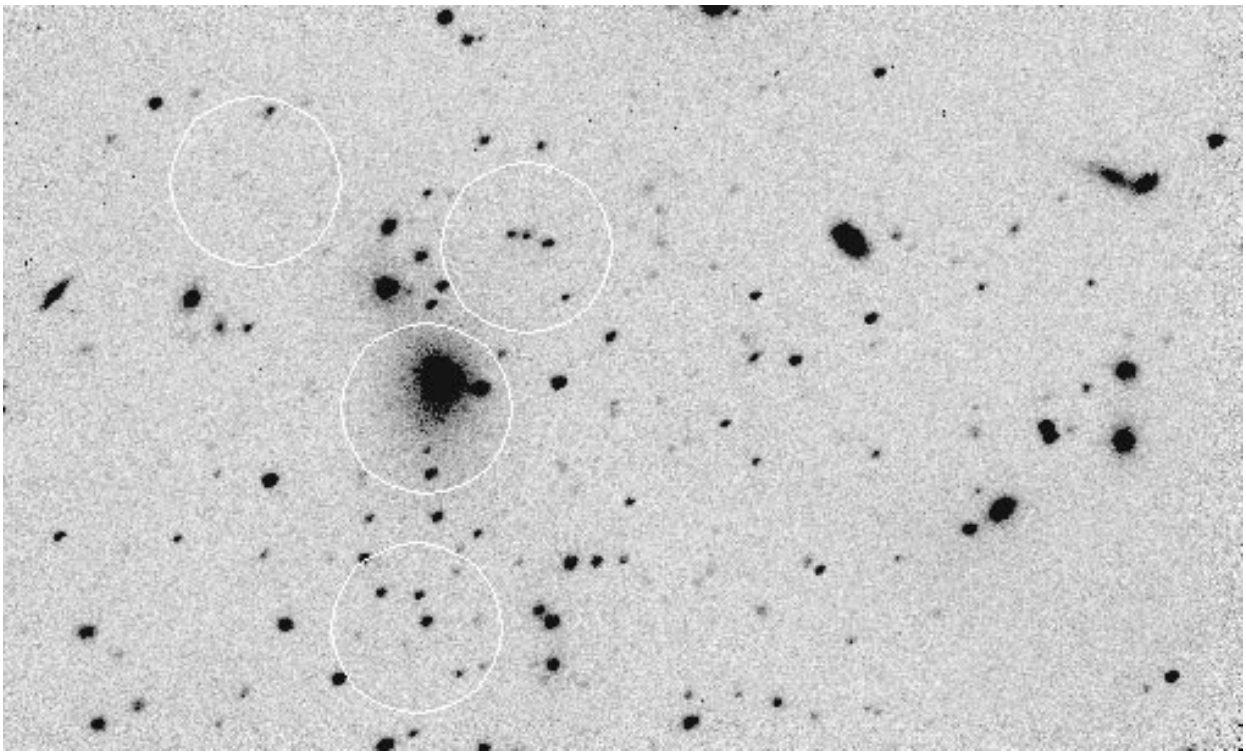

FIG. 1*b*

FIG. 1.—Tesselated *R*-band CCD data of the clusters Abell 115 (*a*), Abell 403 (*b*), and Abell 2397 (*c*), also showing the location of the IR apertures. The intensity scale is linear in photographic density where $\mu_R = 20.5$ is black and $\mu_R = 21.0$ is white.

spread in the colors (standard deviation) of the survey galaxies.

The $B-V$, $V-K$, and $J-K$ colors of the cluster positions are consistent with standard E/S0 colors, except for position 4 of Abell 403 which is somewhat redder. However, even the largest discrepancy, the $V-K$ color, is only off by 3 σ which, given that the errors are a combination of statistical and systematic components, is to be expected. The $B-V$ and $J-K$ colors are even less discrepant. This is shown in Figure 2 which is a plot of the absolute V and K magnitudes for the 15 positions in the seven clusters for which there is a detectable level of V-band light. The solid line indicates the average $V-K$ color of nearby E/S0 galaxies.

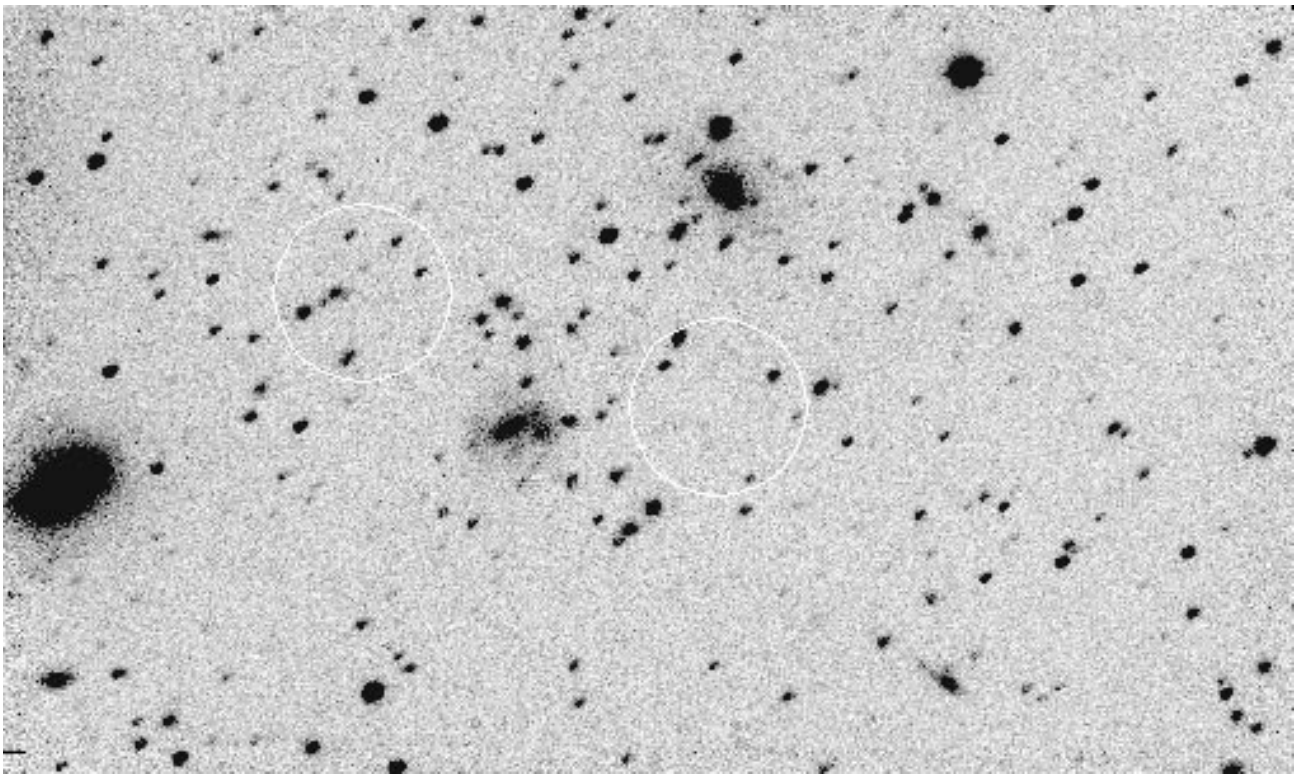

FIG. 1*c*

All of the clusters lie at moderate Galactic latitudes, $b \geq 40°$, so Galactic extinction is not expected to be large. Using the H I dust correlation of Burstein & Heiles (1978), the predicted $V-K$ reddening of the seven clusters ranges from 0.00 to 0.18 mag with the largest correction applying to A403. Because of the uncertainty of the extinction corrections and because they have an insignificant effect on the conclusions of this paper, we have chosen not to correct the data for Galactic extinction.

3.3. *Contamination by Stars and Galaxies*

We estimated the effect of background galaxies using the galaxy number-counts of Tyson & Jarvis (1979) and Kron (1980) and of foreground stars using the predicted star counts of Bahcall & Soneira (1981). The expected contribution of these two classes of sources is less than the uncertainty in the measurements in all cases.

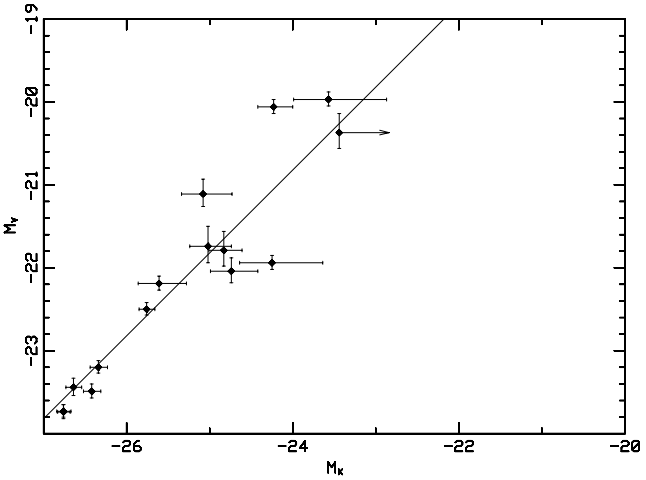

FIG. 2.—Derived V and K absolute magnitudes. The K-corrections assumed that $q_0 = 0$ (see text). No detections were made at positions A403 No. 3 and A1413 No. 2, and these have been left out.

4. DISCUSSION

4.1. *Cluster Masses*

In order to determine the mass-to-light ratios of the clusters, the projected surface mass densities must be estimated as a function of cluster position. For an isothermal King distribution (King 1972) of galaxies, the surface density is well described by

$$\sigma(r) = \frac{2\rho_0 r_c}{(1 + r^2/r_c^2)} \tag{1}$$

where r_c is the core radius, the central density is $\rho_0 = 9V_r^2/4\pi G r_c^2$, V_r is the line-of-sight velocity dispersion, and G is the gravitational constant. This model assumes that dark matter is distributed smoothly with the same core radius as that of the distribution of galaxies. Typical core radii of rich clusters of galaxies are on the order of $0.2\ h^{-1}$ Mpc (Sarazin 1986); however, the surface density near one core radius is not particularly sensitive to r_c. For example, the surface density at $r = 0.2$ Mpc changes by only 20% as r_c is varied between 0.1 and 0.4 Mpc.

On the other hand, recent observations of gravitationally lensed arcs indicate that the dark matter in clusters of galaxies may be significantly more centrally condensed than the galaxies with dark matter core radii as small as $25\ h^{-1}$ kpc (Miralda-Escude 1995; Wallington, Kochanek, & Koo 1995; Kneib & Soucail 1996). Such a possibility was considered by Bailey (1982) who evaluated the mass required to bind an approximately isothermal distribution of galaxies

TABLE 3

CORRECTED COLORS

Cluster	$B-V$	$V-K$	$J-K$
A115 No. 1	0.85 ± 0.11	3.14 ± 0.13	1.03 ± 0.16
A115 No. 2	0.55 ± 0.30	...	...
A115 No. 3	0.65 ± 0.13	$2.31^{+0.42}_{-0.61}$	$1.81^{+3.20}_{-0.95}$
A403 No. 1	0.88 ± 0.11	3.26 ± 0.13	0.63 ± 0.14
A403 No. 2	1.03 ± 0.17	$3.60^{+0.44}_{-0.71}$	1.33 ± 0.83
A403 No. 3	...	...	...
A403 No. 4	1.54 ± 0.20	4.17 ± 0.22	$2.16^{+0.94}_{-0.54}$
A910 No. 1	0.92 ± 0.15	2.93 ± 0.14	0.85 ± 0.17
A910 No. 2	$0.93^{+0.60}_{-0.43}$	3.28 ± 0.33	0.55 ± 0.38
A1413 No. 1	0.89 ± 0.12	3.03 ± 0.12	0.92 ± 0.12
A1413 No. 2	...	...	...
A1763 No. 1	0.87 ± 0.16	3.20 ± 0.15	1.16 ± 0.14
A1763 No. 2	0.73 ± 0.36	3.04 ± 0.30	$1.29^{+0.45}_{-0.36}$
A2218 No. 1	0.85 ± 0.12	3.02 ± 0.12	0.87 ± 0.12
A2218 No. 2	0.86 ± 0.18	2.70 ± 0.32	0.53 ± 0.36
A2397 No. 1	$0.98^{+0.33}_{-0.28}$	$3.97^{+0.31}_{-0.39}$	$0.39^{+0.36}_{-0.41}$
A2397 No. 2	1.16 ± 0.17	$3.42^{+0.27}_{-0.34}$	$0.79^{+0.37}_{0.40}$
Median of clusters	0.88	3.17	0.90
Average E/S0	0.93 ± 0.15	3.18 ± 0.21	0.82 ± 0.07

under a variety of assumptions about the shape of the dark matter profile and the value of the core radius. Using Bailey's results we have shown that the projected surface density of dark matter at positions within 0.2 h^{-1} Mpc, i.e., one galaxy-cluster core radius, of the center is not very sensitive to the dark matter distribution (UB91). In the most extreme cases, the value of the projected surface density at a radius of 0.2 h^{-1} Mpc is only 30% less than that predicted by the isothermal King distribution of equation (1). In general, the more centrally condensed models have surface densities in excess (up to a factor of two) of the King distribution inside one core radius (UB91). All 17 of the clusters positions listed in Table 3 are within 0.2 h^{-1} Mpc of the cluster center.[3]

As a specific example, consider the two-dimensional Newtonian potential

$$\phi(r) = A(1 + r^2/s^2)^{1/2} , \quad (2)$$

discussed by Kochanek & Blandford (1987), where s is the dark matter core radius. This potential approximates that of a singular isothermal sphere at large radii. Kochanek & Blandford showed that the central surface density required to bind an isothermal galaxy distribution with radial velocity dispersion V_r^2 is

$$\sigma_0 = V_r^2/Gs , \quad (3)$$

where G is again the gravitational constant. If $s = 25\ h^{-1}$ kpc, then the effective radius of our aperture is typically $3s$. The mass enclosed by this aperture at the center of the cluster corresponds to an average central surface density of $\langle\sigma\rangle \approx 0.316V_r^2/Gs$. For comparison, a similar calculation for the isothermal King distribution with $r_c = 8s = 200\ h^{-1}$ kpc results in a central average surface density of $\langle\sigma\rangle_{\rm King} \approx 1.32V_r^2/Gr_c$ or about a factor of 2 smaller than that of the two-dimensional Newtonian model. At distances of 0, 50, 100, 150, and 200 h^{-1} kpc from the cluster center, the range of positions for the present observations, the ratios of the average surface density of the two-dimensional Newtonian model to the isothermal King model are 1.9, 1.7, 1.1, 0.78, and 0.74, respectively. Near the center of the cluster, the King model underestimates the masses with respect to the Newtonian model. Outside five dark matter core radii, the King model overestimates the mass but only by 35% in the worst case (at $8s$ or $1r_c$).

Models of gravitational lens provide independent estimates of cluster masses. In general, lensing masses are in agreement with dynamical masses (Wu & Fang 1997; Kneib & Soucail 1996; Miralda-Escudé & Babul 1995; Miralda-Escudé 1995; Wallington et al. 1995). As an example, consider the excellent lens model of Abell 2218 which was based on *HST* observations (Kneib et al. 1996). This lens model predicts beam-averaged surface densities within 0.2 h^{-1} Mpc of from 1.5 to 0.9 times those computed from a King model with a velocity dispersion of 1200 km s^{-1} and a core radius of 0.2 h^{-1} Mpc (the model we used in UB91). As with the two-dimensional Newtonian model the lens model predicts a significantly higher central surface density.

On the other hand, it has been pointed out that cluster masses determined from the temperature and distribution of X-ray–emitting gas are from 2 to 3 times smaller than masses implied by dynamics and lenses (Wu & Fang 1997; Miralda-Escudé & Babul 1995). Again we consider A2218 as an example. Using a β model (see, for example, Sarazin 1986) for the X-ray–emitting gas with $\beta = 0.71$ and $r_c = 138\ h^{-1}$ kpc (Squires et al. 1996) we have computed the mass column density following Wu (1994). Taking the X-ray temperature to be the average of that obtained by *ASCA* (Yamashita 1995) and *Ginga* (McHardy et al. 1990), i.e., 7.4 keV, this model predicts beam averaged surface densities within 0.2 h^{-1} Mpc of 0.8 ± 0.1 times those computed from a King model with a velocity dispersion of 1200 km s^{-1} and a core radius of 0.2 h^{-1} Mpc (again, the model we used in UB91). This agreement is, perhaps, fortuitous, and we do not mean to imply that X-ray profiles can be used to reliably infer cluster masses. However, this example once again illustrates that surface densities within an optical core radius are much less sensitive to the dark matter model than is the total mass.

The result of these considerations is that we have chosen to use the King profile with $r_c = 0.2\ h^{-1}$ Mpc since it provides the more conservative estimate near the cluster center while it is not significantly different from more centrally condensed models at larger distances. It seems unlikely that the resulting mass estimates within one optical core radius are wrong by more than a factor of 2 (except at the cluster center where the King model results in a more conservative estimate) unless current understanding of cluster masses is found to be seriously in error.

The line-of-sight velocity dispersion for A115 was measured by Beers et al. (1983). They found that A115 contains two main subclusters. We centered our observations on the southern subcluster (B in their notation) and adopted a line-of-sight rms velocity of 1130 km s^{-1}, derived from the measured redshifts of the galaxies in this clump. Using the temperature/velocity dispersion relation of White & Fabian (1995), this velocity is consistent with the temperature of the X-ray–emitting gas in the cluster (Worrall, Birkinshaw, & Cameron 1995; Ebeling et al. 1996). There is no published velocity dispersion of A2397; however, the X-ray temperature (Wang & Stocke 1993) implies an rms velocity dispersion of 1000 km s^{-1} and the gravitational lens arc in

[3]We assume an open universe, $q_0 = 0$; however, the mass-to-light ratios in Table 4 below actually increase by $\sim 10\%$ for a $q_0 = 0.5$ universe.

TABLE 4

MASSES AND MASS-TO-LIGHT RATIOS[a]

Cluster Positions	Mass ($10^{13}\ h^{-1}\ M_\odot$)	$(M/L)_B\ h^{-1}$	$(M/L)_V\ h^{-1}$	$(M/L)_J\ h^{-1}$	$(M/L)_K\ h^{-1}$
A115 No. 1	3.90	290	240	91	49
A115 No. 2	3.00	2200	2400	>590[b]	>540[b]
A115 No. 3	3.20	620	620	>530[b]	280
A403 No. 1	0.97	140	110	32	21
A403 No. 2	0.84	1400	1000	400	140
A403 No. 3	0.68	2300	>17000[b]	>210[b]	>170[b]
A403 No. 4	0.78	2000	860	>280[b]	70
A2397 No. 1.....	2.60	1500	1100	110	100
A2397 No. 2.....	2.30	580	360	90	60

[a] We use solar units for each band.
[b] The lower limits are 1 σ upper limits to the luminosity, see Table 1.

that cluster is consistent with this value (Kneib & Soucail 1996). We could locate no published values for velocity dispersion, lensing model, nor X-ray temperature for A403; however, rich Abell clusters typically have velocity dispersions in excess of 1000 km s^{-1} (Bahcall 1981) with values ranging up to 1400 km s^{-1} (Dressler 1981). Therefore, we assume a value of 1000 km s^{-1} for this cluster.

While it has been agued that the dark matter in clusters cannot be associated with individual galaxies because such massive objects would have collapsed to the cluster center through dynamical friction (Sarazin 1986), it is still possible that the dark matter is not smoothly distributed as we have assumed above but rather is somewhat clumped (Tyson 1996). Indeed, most lensing models indicate some degree of clumping. If this is the case, then the off-cluster mass-to-light ratios derived below are likely to be overestimates in some cases but underestimates in others. At the center positions, on the other hand, the mass-to-light ratios will likely be underestimates for reasons stated above.

Table 4 lists the projected masses and B-, V-, J-, and K-band mass-to-light ratios for the nine cluster positions in Table 1. An open ($q_0 = 0$) cosmology was assumed. A flat universe ($q_0 = 0.5$) would imply slightly larger (up to 10%) mass-to-light ratios than those listed in Table 4. We have made no attempt to estimate errors for these values because of the uncertainties in the distribution of dark matter. We estimate that individual entries are probably accurate to within a factor of 2.

4.2. *Colors and Magnitudes of 0.1 $M_\odot$ Stars*

If a major component of the dark matter in clusters of galaxies consists of low-mass dwarfs, it seems reasonable to assume that they would be an old population with low metallicity ($Z < 0.001$). Since the mass function of such objects is unknown, we have chosen to constrain models by considering a population which consists entirely of 0.1 $M_\odot$ stars, i.e., late M subdwarfs. The constraint can then be expressed as the maximum fraction of the dark matter than can be in the form of stars with masses $\geq 0.1\ M_\odot$. We chose this way to constrain the mass function because it is the most conservative, i.e., any mass function which requires stars more massive (and brighter) than 0.1 $M_\odot$ results in a stronger constraint.

The colors and magnitudes of a 0.1 $M_\odot$ subdwarf are uncertain due to our lack of knowledge of the mass-luminosity relation of such stars. From Saumon et al. (1994) it seems likely that the bolometric magnitude of a 0.1 $M_\odot$, low-metallicity ($Z < 0.001$) dwarf is within a few tenths of a magnitude of $M_{\rm bol} = 11.6$. We estimated M_I and M_K from the rather tight relation between $M_{\rm bol}$ and M_I, M_K derived from infrared observations high proper motion subdwarfs (Greenstein 1989). The $V-K$ and $V-R$ colors were estimated from the correlation of these quantities with $M_{\rm bol}$; although in these cases the correlations are less tight (corrections of 0.2 mag were applied to the V and I magnitudes to transform these to the Kron-Cousins system). The resulting magnitude and colors of this hypothetical 0.1 $M_\odot$ subdwarf are listed in Table 5. It is interesting to note that these values are within 0.1 mag of those of the subdwarf LHS 1970 (Monet et al. 1992) which Saumon et al. (1994) suggest is an extreme subdwarf with mass of about 0.1 $M_\odot$. The colors are also consistent with halo stars of comparable magnitude in the dwarf star survey of Leggett (1992).

Although the uncertainties in the subdwarf magnitudes should be considered to be of the order of half a magnitude, this translates into an error in the mass of less than 10% because of the large slope of the mass-luminosity relation (Saumon et al. 1994). Indeed, the model of Baraffe & Chabrier (1996) for a $Z = 6 \times 10^{-4}$, 0.1 $M_\odot$ star is about 0.3 mag fainter than those in Table 5 in M_V and M_I, while the $Z = 1 \times 10^{-4}$ model of D'Antona & Mazzitelli (1996) is about 0.6 mag dimmer in these bands. Nevertheless, the corresponding magnitudes for 0.11 $M_\odot$ stars for these models are brighter than those listed in Table 5. Therefore, uncertainties in subdwarf magnitudes and colors translate into an uncertainty in the mass constraints (see § 4.3) of $\leq 10\%$.

Also listed in Table 5 are the magnitudes of the zero-metallicity model of Saumon et al. (1994). For comparison, we have also included the corresponding values for an old disk ($Z \leq 0.01$) dwarf of the same mass. The latter magnitudes are the averages of those of M5.5 and M6 dwarfs

TABLE 5

MAGNITUDE AND COLORS OF 0.1 $M_\odot$ DWARFS

Parameter	($Z = 0$) Dwarf	Subdwarf	Old Disk Dwarf
$M_{\rm bol}$	11.4	11.6	12.1
M_K.....	9.7[a]	8.8	9.2
M_I	10.5	11.1	12.3
M_R.....	11.3	12.1	14.4
M_V.....	12.0	13.3	16.2
$V-K$.....	2.3	4.5	7.0
$V-I$.....	1.5	2.2	3.9
$V-R$	0.7	1.2	1.8

[a] The K-band luminosity of this star is suppressed by H^2 opacity (Saumon et al. 1994).

(Bessell 1991). From the mass-luminosity relations of Henry & McCarthy (1993), we conclude that the average mass of these stars, is indeed, 0.1 $M_\odot$.

Stars at the edge of the main sequence are somewhat less massive and much less luminous than the canonical 0.1 $M_\odot$ dwarfs listed in Table 5. In terms of such "edge dwarfs" the constraints that we derive in § 4.3 below would be less stringent. Furthermore, the luminosities of dwarfs with masses only 30% smaller (brown dwarfs) are so low that our observations pose no constraints whatsoever on such objects. However, the purpose of this paper is not to determine whether or not edge dwarfs are a significant component of dark matter but rather to constrain the mass function of a hypothetical dwarf population. There seems to be no a priori reason for a relation between the critical mass for hydrogen burning and the stellar mass function; in particular, it seems unlikely that the mass function would be discontinuous just below 0.1 $M_\odot$. For this reason we choose to express our limits as constraints on stars with 0.1 $M_\odot$ in the following section.

4.3. *Dark Matter Constraints*

As is apparent in Table 5, the $V-K$ colors of subdwarfs and old disk dwarfs are considerably redder than that of a typical galaxy (see Table 3), while the $V-K$ color of the zero metallicity dwarf is bluer than that of galaxies. An upper limit to the contribution of dwarfs to the dark matter can be derived by computing the maximum mass which could be contributed by such stars without resulting in galaxy colors which differ significantly from those measured.

Consider a population of dwarfs. Since the light from this population must be K-corrected differently than ordinary galaxy light, we proceed as follows. The light of the hypothetical dwarf population is "K-corrected" to the observer's frame and subtracted from the observed cluster light. The residual flux is then K-corrected back to the cluster frame assuming it has the canonical galaxy specrum. If the color of the residual cluster light is significantly different from the canonical galaxy color, then the hypothetical dwarf population is inconsisent with the observations.

For example, Figure 3 is a plot of the corrected absolute V and K magnitudes of the cluster positions under the assumption that 10 h^{-1}% of the dark matter consists of 0.1 $M_\odot$ subdwarfs. It is quite evident that the corrected cluster colors are inconsistent with typical galaxy colors. Indeed, 10 of the 14 plotted points fall on the blue side of the $V-K=3.18$ galaxy curve. For the three cluster positions not plotted in Figure 3 (A115 No. 2, A403 No. 3, see Table 3; A1413 No. 2, see UB91), the lack of any observed K-band light implies 1 σ limits of 3 h^{-1}%, 9 h^{-1}%, and 3 h^{-1}% on the subdwarf content of dark matter. Therefore, 13 of the 17 observed positions are inconsistent with the hypothesis that 10 h^{-1}% of the dark matter in these clusters consists of a population of 0.1 $M_\odot$ subdwarfs.

It could be argued that evolutionary effects in the normal stellar populations might result in an anomalous blue color which might mask a red component. However, the redshifts of these clusters are modest ($0.11 \le z \le 0.22$) and anomalously blue ($V-K$) colors of the central regions of individual galaxies have not been observed at these redshifts. In addition, the cores of the brighter galaxies in these clusters have $V-K$ colors consistent with those of nearby E and S0 galaxies. We therefore conclude that the hypothesis that 10 h^{-1}% of the dark matter is in the form of 0.1 $M_\odot$ subdwarfs is strongly rejected.

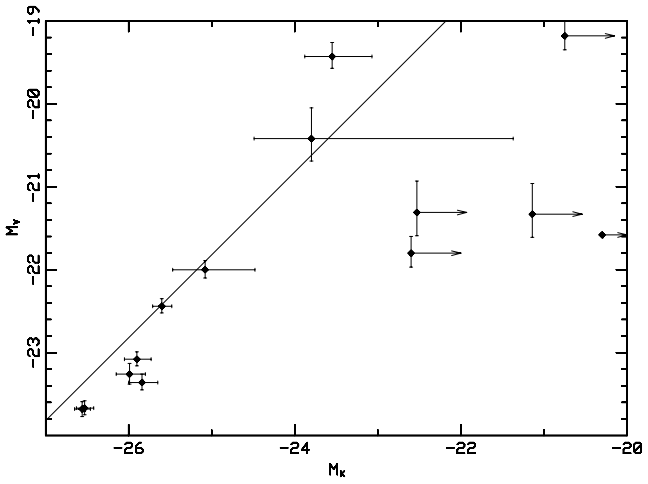

FIG. 3.—Corrected absolute V and K magnitudes assuming that 10 h^{-1}% of the dark matter is in the form of 0.1 $M_\odot$ subdwarfs. The corrected K-band light for A115 No. 3 is more than 1 σ negative. This value is plotted as an arrow at the right of the figure at the appropriate M_V level. For A115 No. 2, both the corrected V- and K-band light are negative, so this cluster is omitted from the figure.

Another way to contrain the infrared emission of the dark matter is to use the V-band flux to determine the constribution of the ordinary stellar population and then correct the K band light accordingly. This is possible since the $V-K$ color of 0.1 $M_\odot$ subdwarfs, $V-K=4.5$, is much larger than that of the ordinary stellar population, $V-K=3.2$. This implies that, per unit of K-band flux, the ordinary stellar population is more than 3 times brighter in the V band than is the hypothetical subdwarf population.

Let F_K and F_R be the observed K- and R-band fluxes with $F_{K,G}$ and $F_{R,G}$ the fluxes due to the normal stellar populations in galaxies and $F_{K,D}$ and $F_{R,D}$ the K- and R-band fluxes due to the dark matter. The luminosity corresponding to a given flux is $L=AF$, where $A=4\pi d_L^2 10^{0.4\Delta}$, d_L is the luminosity distance and Δ is the K-correction. The K-band flux due to dark matter is then given by

$$F_{K,D}=F_K-F_{K,G}=F_K-\frac{L_{K,G}}{A_{K,G}}. \tag{4}$$

But $L_{K,G}=C_G L_{V,G}$ and $L_{K,D}=C_D L_{V,D}$ where C_G is the factor that corresponds to the nominal color ($V-K=3.2$) for E/S0 galaxies and C_D is the corresponding one for 0.1 $M_\odot$ subdwarfs ($V-K=4.5$). Thus

$$F_{K,D}=F_K-\frac{C_G L_{V,G}}{A_{K,G}}=F_K-C_G\frac{A_{VR,G}}{A_{K,G}}F_{R,G}, \tag{5}$$

where it should be noted that we are transforming the R-band flux to a V-band luminosity, i.e.,

$$L_V=A_{VR}F_R. \tag{6}$$

Now

$$F_{R,G}=F_R-F_{R,D}, \tag{7}$$

so that

$$F_{K,D}=F_K-C_G\frac{A_{VR,G}}{A_{K,G}}F_R+\frac{C_G A_{VR,G}A_{K,D}}{C_D A_{K,G}A_{VR,D}}F_{K,D}. \tag{8}$$

Solving for $F_{K,D}$

$$F_{K,D} = \frac{F_K - C_G F_R A_{VR,G}/A_{K,G}}{1 - [(C_G A_{VR,G} A_{K,D})/C_D A_{K,G} A_{VR,D})]} \quad (9)$$

Finally, we can express the K-band light-to-mass ratio of the dark matter, $L_{K,D}/M$, as a function of the K- and R-band fluxes as

$$\frac{L_{K,D}}{M} = \frac{A_{K,D}(F_K - C_G F_R A_{VR,G}/A_{K,G})}{M\{1 - [(C_G A_{VR,G} A_{K,D})/(C_D A_{K,G} A_{VR,D})]\}} \quad (10)$$

Table 6 is a list of the light-to-mass ratios obtained in this way for the 17 individual cluster positions expressed in solar K-band units. The errors quoted are quadrature combinations of the statistical errors in F_R and F_K, the 20% variation in C_G due to the spread in $V-K$ colors of normal galaxies, and the 11% variation in $A_{VR,G}/A_{K,G}$ due to uncertainties in calibration and K-corrections, all multiplied by the appropriate factors indicated in equation (10). Since no R-band light was observed for positions A403 No. 3 and A1413 No. 2, the values are those obtained from the K-band measurements alone. Therefore, these two entries represent upper limits. The reduced χ^2 for these points is 1.3 (0.9, if the most discrepant point is removed). The largest deviation, which corresponds to position A403 No. 4 is only 2.8 σ. Given that the errors include a contribution from systematic effects, the distribution and χ^2 are reasonable. The distribution is consistent with a light-to-mass ratio of zero. For comparison the K-band light-to-mass ratio of the 0.1 $M_\odot$ subdwarf of Table 5 is $(L/M)_K = 0.07(L_\odot/M_\odot)_K$. The 1 σ upper limit on the straight average from the positions in Table 6 is 2 h^{-1}% of this value while the weighted average corresponds to 1 h^{-1}%. We therefore, conclude that no more than 2 h^{-1}% of the dark matter in the clusters can be in the form of 0.1 $M_\odot$ subdwarfs. Using only the data on A115, A403, and A2397 yields a limit of 4 h^{-1}%.

Also listed in Table 6 are the residual light-to-mass ratios under the assumption that the dark matter has the colors of the 0.1 $M_\odot$ old disk dwarf listed in Table 5. The K-band light-to-mass ratio for this star is $0.05(L_\odot/M_\odot)_K$ and the 1 σ upper limits on the straight and weighted averages correspond to 2 h^{-1}%. Again, we conclude that no more than 2 h^{-1}% of the dark matter in the clusters can be in the form of 0.1 $M_\odot$ old disk dwarfs.

The analysis for a zero metallicity dwarf is somewhat different since such a star is predicted to be bluer in $V-K$ than E/S0 galaxies. In this case one can use the K-band flux to determine the contribution of the ordinary stellar population and then correct the R-band light accordingly. The result is the same as that of equation (10) but with the roles of VR and K interchanged. The last column in Table 6 lists the residual V-band light-to-mass ratios under the assumption that the dark matter has the colors of the zero metallicity model in Table 5. Since no K-band light was observed for cluster positions A115 No. 2, A403 No. 3, and A1413 No. 2, the values listed are obtained from R-band measurements alone. Those three entries might still contain contributions from galaxy light and therefore represent upper limits. The errors for those points are quite small since they represent the measurement noise for the R-band photometry. For this reason we only use the straight average for this column. The V-band light-to-mass ratio for the zero-metallicity model dwarf is $0.014(L_\odot/M_\odot)_V$. The 1 σ upper upper limit on the straight average in Table 6 corresponds to 3 h^{-1}% of this value, which implies that at most 3 h^{-1}% of the dark matter in these clusters can be in the form of 0.1 $M_\odot$ zero-metallicity stars.

All of the above limits rely on using color differences to distinguish the hypothetical dwarf population from the normal stellar population of E/S0 galaxies. As shown in Table 5, low-metallicity 0.1 $M_\odot$ subdwarfs are redder in $V-K$ than the normal stellar population while zero-metallicity dwarfs are somewhat bluer. Therefore, it is possible that dwarfs with some intermediate metallicity between the ones we have considered might have $V-K$ color identical to that of the normal stellar population.

TABLE 6

LIGHT-TO-MASS RATIOS

Cluster	Sudwarf $(L/M)h$[a]	Old Disk Dwarf $(L/M)h$[a]	$Z = 0$ Dwarf $(L/M)h$[b]
A115 No. 1	$(-12 \pm 69) \times 10^{-4}$	$(-9 \pm 52) \times 10^{-4}$	$(3 \pm 18) \times 10^{-4}$
A115 No. 2	$(-48 \pm 30) \times 10^{-4}$	$(-36 \pm 22) \times 10^{-4}$	$(4 \pm 1) \times 10^{-4}$
A115 No. 3	$(-69 \pm 36) \times 10^{-4}$	$(-52 \pm 26) \times 10^{-4}$	$(19 \pm 9) \times 10^{-4}$
A403 No. 1	$(56 \pm 154) \times 10^{-4}$	$(39 \pm 106) \times 10^{-4}$	$(-12 \pm 34) \times 10^{-4}$
A403 No. 2	$(39 \pm 61) \times 10^{-4}$	$(27 \pm 42) \times 10^{-4}$	$(-8 \pm 13) \times 10^{-4}$
A403 No. 3	$(10 \pm 50) \times 10^{-4}$	$(11 \pm 53) \times 10^{-4}$	$(-1 \pm 1) \times 10^{-4}$
A403 No. 4	$(144 \pm 51) \times 10^{-4}$	$(99 \pm 32) \times 10^{-4}$	$(-30 \pm 15) \times 10^{-4}$
A910 No. 1	$(-66 \pm 68) \times 10^{-4}$	$(-50 \pm 51) \times 10^{-4}$	$(18 \pm 16) \times 10^{-4}$
A910 No. 2	$(10 \pm 39) \times 10^{-4}$	$(8 \pm 29) \times 10^{-4}$	$(-3 \pm 11) \times 10^{-4}$
A1413 No. 1	$(-85 \pm 133) \times 10^{-4}$	$(-61 \pm 95) \times 10^{-4}$	$(19 \pm 27) \times 10^{-4}$
A1413 No. 2	$(8 \pm 12) \times 10^{-4}$	$(8 \pm 13) \times 10^{-4}$	$(1 \pm 1) \times 10^{-4}$
A1763 No. 1	$(4 \pm 50) \times 10^{-4}$	$(3 \pm 37) \times 10^{-4}$	$(-1 \pm 13) \times 10^{-4}$
A1763 No. 2	$(-13 \pm 33) \times 10^{-4}$	$(-10 \pm 25) \times 10^{-4}$	$(3 \pm 8) \times 10^{-4}$
A2218 No. 1	$(-103 \pm 153) \times 10^{-4}$	$(-76 \pm 112) \times 10^{-4}$	$(25 \pm 33) \times 10^{-4}$
A2218 No. 2	$(-69 \pm 56) \times 10^{-4}$	$(-51 \pm 40) \times 10^{-4}$	$(17 \pm 12) \times 10^{-4}$
A2397 No. 1	$(78 \pm 45) \times 10^{-4}$	$(60 \pm 34) \times 10^{-4}$	$(-23 \pm 16) \times 10^{-4}$
A2397 No. 2	$(53 \pm 82) \times 10^{-4}$	$(41 \pm 63) \times 10^{-4}$	$(-16 \pm 26) \times 10^{-4}$
Straight average[c]	$(-3.7 \pm 15.9) \times 10^{-4}$	$(-2.9 \pm 11.5) \times 10^{-4}$	$(0.9 \pm 3.8) \times 10^{-4}$
Weighted average[d]	$(1.2 \pm 8.6) \times 10^{-4}$	$(0.3 \pm 7.5) \times 10^{-4}$	$(1.4 \pm 0.6) \times 10^{-4}$

[a] Solar K-band units.
[b] Solar V-band units.
[c] Error computed from the distribution of the data.
[d] Error computed from the errors in the data.

However, it is unlikely that other colors (such as $V-R$) would also be the same. Nevertheless, without a specific model it is not possible to use color information to limit such a hypothetical population. An upper limit to the fraction of the dark matter that could be packed in such a "worst case" subdwarf can be obtained by assuming that all the light in the 'off-center" cluster positions is due to such a population. The average of the K-band light-to-mass-ratios of the 11 off center cluster positions is 7.5×10^{-3} in solar units. We estimate the K-band luminosity of this "worst-case" subdwarf by taking the average of the values that correspond to the ordinary 0.1 $M_{\odot}$ subdwarf and the zero-metallicity dwarf listed in Table 5, which yields a light-to-mass ratio of 0.05 in solar K-band units for this hypothetical star. Therefore, no more than 15 h^{-1}% of the dark matter could be in the form of this "worst-case" 0.1 $M_{\odot}$ subdwarfs. The R-band light-to-mass ratios yield a similar limit. For the darkest seven (of 11) off-center-position, this limit decreases to $\sim 10\, h^{-1}$%.

Finally, we consider the possibility that the dark matter is not smoothly distributed but is somewhat clumped (Tyson 1996). Although this should not affect the derived light-to-mass ratios for the six central cluster positions, any of the 11 off-center positions might be located in a region with lower than expected dark matter density. Since the above limits result from an average of 11 cluster positions with diameters of order 100 kpc, we believe them to be reasonably insensitive to some dark matter clumping. The clumping would have to be extreme, with the dark matter contained in less than 3% of the cluster volume, so that all 11 of our off beams had been placed in the voids between the dark matter clumps. In such a scenario, only the seven central cluster positions would be sensitive to dark matter luminosity and the above limits would have to be increased by about a factor of 2. We believe that such an extreme case is rather unlikely.

5. CONCLUSIONS

After correcting for the light of the standard stellar population in E/S0 galaxies, the residual K- and V-band light at positions near the cores of seven rich Abell clusters is consistent with zero. These corrections require the knowledge of the color of any light associated with the dark matter. We have assumed three model populations of 0.1 $M_{\odot}$ dwarf stars: the zero-metallicity model of Saumon et al. (1994), observed extreme subdwarfs, and observed old disk dwarfs. Our data limit the 0.1 $M_{\odot}$ dwarf content of the dark matter to $\leq 2\, h^{-1}$% to 3 h^{-1}% of the mass required by cluster dynamics, depending on the actual population assumed. Even if the dark component is assumed to have colors identical to those of the ordinary stellar content of the E/S0 galaxies in the clusters, these limits only increase to ~ 10 h^{-1}%.

These limits do not include an account for the errors in the estimate of the masses of the clusters. We have shown that the surface mass density within one optical core radius is much less sensitive to the profile of the dark matter than is the total cluster mass and it seems unlikely that the error estimated the surface mass density would change the entries in Table 6 by more than a factor of 2 unless the dark matter is significantly clumped. In any case, the mean light-to-mass in Table 6 should not be overly sensitive to this effect since our limits are not derived from the position with the lowest light-to-mass ratio but follow from a statistical ensemble of measurements at 17 distinct but similar cluster positions. Unless the current understanding of the masses of clusters of galaxies is in serious error, we consider that the above limits are good to within a factor of 2.

The limits derived in this paper do not rule out brown dwarfs as the primary constituent of dark matter in clusters of galaxies. However, they do place a significant constraint on the subdwarf mass function which would have to rise sharply below 0.1 $M_{\odot}$ if subdwarfs comprise the bulk of the dark matter.

We acknowledge helpful discussions with Adam Burrows, Jay Gallagher, Dick Joyce, Jeff Kuhn, Richard Larson, Jim Peebles, and Ron Probst. We thank the staff at KPNO for their support with these observations. This work was supported in part by the Gravitation research group at the Physics Department of Princeton University, and we thank Ed Groth and Dave Wilkinson for their support. This research was supported in part by the National Science Foundation (grant PHY-9222952) and the Monell Foundation.

REFERENCES

Aaronson, M. 1977, Ph.D. thesis, Harvard Univ.
Aaronson, M., Persson, S. E., & Frogel, J. A. 1981, ApJ, 245, 18
Bahcall, N. A. 1981, ApJ, 247, 787
Bahcall, J. N., & Soneira, R. A. 1981, ApJS, 47, 357
Bailey, M. E. 1982, MNRAS, 201, 271
Baraffe, I., & Chabrier, G. 1996, ApJ, 461, L51
Beers, T. C., Huchra, J. H., & Geller, M. J. 1983, ApJ, 264, 356
Bessell, M. S. 1991, AJ, 101, 662
Boughn, S. P., & Saulson, P. R. 1983, ApJ, 265, L55
Boughn, S. P., & Uson, J. M. 1995a, Phys. Rev. Lett., 74, 216
———. 1995b, Phys. Rev. Lett., 74, 3304
Burstein, D., & Heiles, C. 1978, ApJ, 225, 40
D'Antona, F., & Mazzitelli, I. 1996, ApJ, 456, 329
Dressler, A. 1981, ApJ, 243, 26
Ebeling, H., Voges, W., Bohringer, H., Edge, A. C., Huchra, J. P., & Briel, U. G. 1996, MNRAS, 281, 799
Eisenhardt, P. R. M. 1984, Ph.D. thesis, Univ. Arizona
Faber, S. M., & Gallagher, J. S. 1979, ARA&A, 17, 135
Festin, L. 1997, A&A, in press (astro-ph/9701205)
Flynn, C., Gould, A., & Bahcall, J. N. 1996, ApJ, 466, L55
Frogel, J. A., Persson, S. E., Aaronson, M., & Mathews, K. 1978, ApJ, 220, 75
Graff, D. S., & Freese, K. 1996, ApJ, 456, L49
Greenstein, J. L. 1989, PASP, 101, 787
Henry, T. J., & McCarthy, D. W., Jr. 1993, AJ, 106, 773
King, I. R. 1972, ApJ, 174, L23
Kneib, J. P., Ellis, R. S., Smail, I., Couch, W. J., & Sharples, R. M. 1996, ApJ, 471, 643
Kneib, J. P., & Soucail, G. 1996, in IAU Symp. 173, Astrophysical Applications of Gravitational Lensing, ed. C. S. Kochanek & J. N. Hewitt (Dordrecht: Kluwer), 113
Kochanek, C. S., & Blandford, R. D. 1987, ApJ, 321, 676
Kron, R. G. 1980, ApJS, 43, 305
Landolt, A. U. 1983, AJ, 88, 43
Leggett, S. K. 1992, ApJS, 82, 351
Lequeux, J., Fort, B., Dantel-Fort, M., Cuillandre, J.-C., & Mellier, Y. 1996, A&A, 312, L1
McHardy, I. M., Stewart, G. C., Edge, A. C., Cooke, B., Yamashita, K., & Hatsukade, I. 1990, MNRAS, 242, 215
Miralda-Escudé, J. 1995, ApJ, 438, 514
Miralde-Escudé, J., & Babul, A. 1995, ApJ, 449, 18
Monet, D. G., Dahn, C. C., Vrba, F. J., Harris, H. C., Pier, J. R., Luginbuhl, C. B., & Ables, H. D. 1992, AJ, 103, 638
Peebles, P. J. E. 1993, Principles of Physical Cosmology (Princeton: Princeton Univ. Press), 417
Persson, S. E., Frogel, J. A., & Aaronson, M. 1979, ApJS, 39, 61
Rebolo, R., Zapatero Osorio, M. R., & Martin, E. L. 1995, Nature, 377, 129
Sackett, P. D., Morrison, H. L., Harding, P., & Boroson, T. A. 1994, Nature, 370, 441
Sarazin, C. L. 1986, Rev. Mod. Phys., 58, 1
Saumon, D., Bergeron, P., Lunine, J. I., Hubbard, W. B., & Burrows, A. 1994, ApJ, 424, 333

Skrutskie, M. F., Shure, M. A., & Beckwith, S. 1985, ApJ, 299, 303
Squires, G., Kaiser, N., Babul, A., Fahlman, G., Woods, D., Neumann, D. M., & Bohringer, H. 1996, ApJ, 461, 572
Tyson, J. A. 1996, in IAU Symp. 173, Astrophysical Applications of Gravitational Lensing, ed. C. S. Kochanek & J. N. Hewitt (Dordrecht: Kluwer), 107
Tyson, J. A., & Jarvis, J. F. 1979, ApJ, 230, L153
Uson, J. M., & Boughn, S. P. 1991, ApJ, 369, 38 (UB91)
Wallington, S., Kochanek, C. S., & Koo, D. C. 1995, ApJ, 441, 58
Wang, Q., & Stocke, J. T. 1993, ApJ, 408, 71
White, D. A., & Fabian, A. C. 1995, MNRAS, 273, 73
Worrall, D. M., Birkinshaw, M., & Cameron, R. A. 1995, ApJ, 449, 93
Wu, X.-P. 1994, ApJ, 436, L115
Wu, X.-P., & Fang, L.-Z. 1997, ApJ, 483, 701
Yamashita, K. 1995, in Clusters of Galaxies, ed. F. Durret, A. Mazure, & J. T. T. Van (Gif-sur-Yvette Cedex: Editions Frontières), 153
Yee, H. K. C., & Oke, J. B. 1978, ApJ, 226, 753
Zapatero-Osorio, M. R., Rebolo, R., & Martin, E. L. 1997, A&A, 317, 164
Zwicky, F. 1933, Helvetica Phys. Acta, 6, 110